applied sciences

MDPI

Article

Three-Phase Unbalance Analysis Method Based on Three-Phase Motor Current Instantaneous Information

Xun Zhang [1], Guanghua Xu [1,2,*], Xiaobi Chen [1], Ruiquan Chen [1], Shengchao Chen [1] and Sicong Zhang [1]

[1] School of Mechanical Engineering, Xi'an Jiaotong University, Xi'an 710049, China
[2] State Key Laboratory for Manufacturing Systems Engineering, Xi'an Jiaotong University, Xi'an 710049, China
* Correspondence: ghxu@mail.xjtu.edu.cn

Abstract: Motor current signal analysis is a common method that can be applied to the monitoring and diagnosis of electromechanical equipment. Three-phase unbalance will increase the line power loss and affect the safe operation of power-using equipment. To quickly analyze motor current three-phase unbalance, we propose a method to analyze three-phase unbalance by calculating the coefficient of variation of the three-phase current's instantaneous frequency and instantaneous amplitude. Simulations were conducted to analyze the effects of amplitude deviation and phase deviation on the coefficient of variation of instantaneous frequency and instantaneous amplitude. The three-phase unbalance with continuous amplitude change was simulated and its instantaneous performance was analyzed. Experiments were conducted to compare and analyze the instantaneous information characteristics of the motor with the continuous changing of three-phase unbalance under different speed conditions. Simulations and experiments show that the proposed method in this paper can analyze three-phase unbalance.

Keywords: three-phase unbalance; motor current; park vector demodulation; instantaneous frequency; instantaneous amplitude; coefficient of variation

Citation: Zhang, X.; Xu, G.; Chen, X.; Chen, R.; Chen, S.; Zhang, S. Three-Phase Unbalance Analysis Method Based on Three-Phase Motor Current Instantaneous Information. *Appl. Sci.* **2023**, *13*, 6127. https://doi.org/10.3390/app13106127

Academic Editor: Frede Blaabjerg

Received: 5 April 2023
Revised: 9 May 2023
Accepted: 15 May 2023
Published: 17 May 2023

1. Introduction

Motors are widely used in industry. Motors can be divided into DC motors and AC motors according to the type of power supply. Three-phase induction motors are mainly used in CNC machine tools, medical equipment, computer external equipment, and other fields. Thousands of motors fail every year, and a motor failure may affect the operation of a production line. To avoid unexpected motor failures and prevent the loss of production, money, and time, it is reasonable and necessary to develop new technologies and diagnostic systems [1].

Many scholars have already studied methods and techniques for fault detection using vibration signal analysis [2,3], current signal analysis [4], and so on. Motor current signal analysis (MCSA) is a non-invasive method to detect the presence of mechanical and electrical anomalies in motors and driven equipment [5]. For MCSA, many researchers have performed related studies, such as wavelet transform [6,7], neural network [8], singular value decomposition (SVD) [9], etc.

Three-phase power is usually 50/60 Hz frequency with a 120° phase difference, and it is a common source of power for large industrial equipment [10]. For power systems, three-phase balance mainly refers to the equal magnitude of the voltage vectors of the three phases. Three-phase unbalance refers to a power system in which the three-phase current/voltage amplitudes are not consistent, the phase difference is not 120° from each other, and the difference value exceeds the specified range. Three-phase unbalance is a common fault. There are various causes of three-phase unbalance, such as disconnection fault, ground fault, etc. The large imbalance may lead to the instability of electrical equipment operation, resulting in abnormal speed, heat, and other failures. The study of three-phase unbalanced

detection methods is of great significance to improve the operational reliability of industrial equipment [11].

Many researchers have studied the voltage/current three-phase unbalance. Bruzzese, C et al. [12] developed a model based on multiple symmetrical components to detect the lower and upper sidebands of the current fundamental frequency to characterize the broken bars and then analyze the forward and reverse rotational differential frequency of multiple symmetrical components that lead to rotor current imbalance. Sharifi, R et al. [13] used the standard deviation of rotor slot harmonic amplitudes in three-phase currents as an indicator of voltage unbalances and applied it to resistive minor short-circuit faults in the early stages of the fault. Ilamparithi, TC et al. [14] developed a model based on a modified winding function and a finite element-based model to simulate motors with different eccentricity conditions, and experiments were conducted on a three-phase commercial reluctance synchronous motor with medium-to-high eccentricity to reduce the effects of supply imbalance and internal asymmetry and to detect eccentricity using residual cancellation techniques. Bacha, K et al. [15] proposed the Hilbert modulus current space vector and Hilbert phase current space vector as fault features, analyzed the magnitude of the fault-related spectral components via fast Fourier transform (FFT) analysis, and used support vector machine (SVM) for the classification of induction motors for applications, such as voltage unbalance fault detection. Ngote, N et al. [16] proposed a method to apply time-synchronous averaging (TSA) to the Park vector of the stator current to diagnose defects in three-phase wound-rotor induction motors. Elbouchikhi, E et al. [17] proposed calculating the symmetrical components of the stator currents, estimating the power supply fundamental frequency and the three-phase quantities based on the maximum likelihood estimator, and then applying the generalized likelihood ratio test for unbalance fault detection. Sabir, H et al. [18] proposed a monitoring method based on Hilbert transform (HT), TSA, and MCSA, which can detect a small fraction of short-circuit turns in the rotor winding of a wound rotor motor under low or no-load conditions. Khaled Laadjal et al. [19] detected unbalanced supply voltage conditions online by monitoring the relevant indicators calculated by the symmetrical component of the voltage and experimentally verified it under several different operating conditions. Dongare, UV et al. [20] proposed a technique based on the symmetrical component positions of the three-phase rotor currents to form a "wing shape" and investigated the effects of unbalanced stator voltages and structural imbalances, etc. on rotor current measurements.

The existing methods, such as Fast Fourier Transform (FFT), the symmetrical components method, etc. are widely used. FFT is suitable for processing steady-state and periodic signals. For unsteady, aperiodic signals, FFT analysis can produce spectral aliasing and leakage. The symmetrical components method is used to decompose the three-phase voltage/current into positive-sequence, negative-sequence, and zero-sequence components [21]. Moreover, the negative-sequence component and zero-sequence component is obtained for the calculation of unbalance through a vector calculation. The symmetrical components method is only suitable for circuits with linear parameters according to the principle of superposition.

Although the methods mentioned above had been widely used, quick analysis can be further investigated. In this study, to verify the effectiveness of the method, the three-phase unbalanced state caused by amplitude deviation and phase deviation was analyzed by analyzing the instantaneous information characteristics and compared with the symmetrical components method. To analyze the unbalance in the unsteady signal state, the sliding window size is changed and the transient information characteristics performance is analyzed.

This paper proposes a three-phase unbalance analysis method based on three-phase current instantaneous information, by calculating the instantaneous amplitude and instantaneous frequency of three-phase currents and calculating their coefficients of variation

to analyze three-phase unbalance. Then, the coefficient of variation of the instantaneous amplitude and instantaneous frequency is calculated to evaluate the three-phase unbalance.

Key highlights:

(1) The method of the calculation of the instantaneous frequency coefficient of variation and the instantaneous amplitude coefficient of variation to analyze the three-phase unbalance is proposed.
(2) Simulations of the amplitude deviation and phase deviation are carried out, as well as the continuous amplitude change, the effectiveness of the method is verified, and the effects of switching noise and harmonics are analyzed.
(3) Experiment results verify the effectiveness of the method.

Advantages: The instantaneous information of the three-phase current is obtained through Park vector demodulation, the calculation result is similar to the trend of the symmetrical components method, the time complexity of this method is smaller than that of the symmetrical components method, and a smaller sliding window size is required.

Novelty: The instantaneous state change of the measured system is analyzed from the perspective of instantaneous information, and continuous unbalances can also be analyzed. Compared with the symmetrical components method, the proposed method has lower time complexity and a shorter calculation time. There is no requirement for the integer period and its multiple for sliding window selection, and a smaller number of sampling points can be used for analysis.

The remaining sections of this paper are organized as follows. Section 2 illustrates the Park vector demodulation method and the calculation of the coefficient of variation. In Section 3, the simulation verification analyzes the effect of amplitude deviation and phase deviation on three-phase unbalance and its instantaneous information performance. The unbalance of continuous change in amplitude is analyzed, the switching noise addition is carried out, and the effect is analyzed. Simulation of three-phase unbalance using Simulink is realized, and the harmonic effect is analyzed. The experimental verification is carried out to compare and analyze the differences in current instantaneous information of three-phase unbalanced motors at different speeds. The last section is the conclusion.

2. The Proposed Three-Phase Unbalance Analysis Method Based on the Three-Phase Motor Current Instantaneous Information

2.1. General Idea of the Algorithm

To quickly analyze the motor current three-phase unbalance, this paper analyzes the three-phase unbalance from the perspective of instantaneous information (instantaneous amplitude and instantaneous frequency). The flow of the proposed algorithm in this paper is shown in Figure 1.

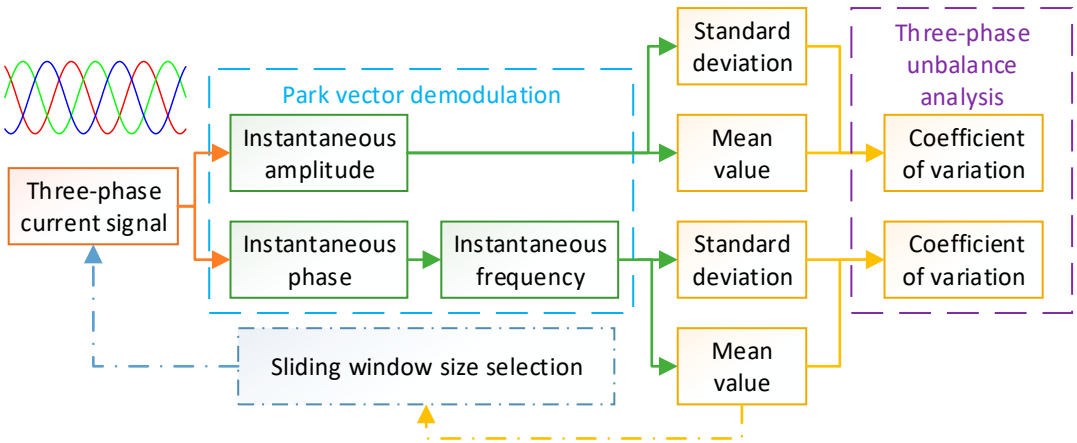

Figure 1. Algorithm flow of the proposed method.

After obtaining the three-phase motor current signal, the instantaneous amplitude and instantaneous phase are calculated based on the park vector demodulation method, and the instantaneous frequency is obtained from the instantaneous phase. The standard deviation and mean value of the instantaneous amplitude and instantaneous frequency are calculated, where the mean value of the instantaneous frequency can be used for the reference of sliding window size selection. The coefficient of variation of the instantaneous amplitude and instantaneous frequency from the standard deviation and mean value are calculated, and the change in the three-phase unbalance is analyzed.

The following subsections introduce the relevant methods and explain them in detail.

2.2. Park Vector Demodulation

The speed of a three-phase asynchronous motor is calculated as shown in Equation (1).

$$n = 60 \cdot \frac{1-s}{p} \cdot f \tag{1}$$

where n is the rotational speed (r/min), s is the slip rate, p is the number of pole-pairs, and f is the rotational frequency.

The three-phase current signal is a modulated signal with a 120° phase difference between any two phases. By using the Park transform, a 90° phase shift signal can be created as a way to complete the signal demodulation [22], as follows.

$$\begin{cases} I_\alpha = \dfrac{2I_u - I_v - I_w}{3} \\ I_\beta = \dfrac{\sqrt{3}(I_v - I_w)}{3} \end{cases} \tag{2}$$

where I_α and I_β are the stator coordinate system currents, and I_u, I_v, and I_w are the motor U-phase, V-phase, and W-phase currents, respectively.

Then, the three-phase current can be expressed as follows:

$$\begin{cases} I_u = a \cdot \cos(2\pi f_M t) \\ I_v = a \cdot \cos\left(2\pi f_M t - \dfrac{2\pi}{3}\right) \\ I_w = a \cdot \cos\left(2\pi f_M t - \dfrac{4\pi}{3}\right) \end{cases} \tag{3}$$

where f_M is the signal fundamental frequency and a is the amplitude of the signal.

Combining Equations (2) and (3) yields the following:

$$\begin{cases} I_\alpha = a \cdot \cos(2\pi f_M t) \\ I_\beta = a \cdot \sin(2\pi f_M t) \end{cases} \tag{4}$$

The analytic signal is constructed from I_α and I_β, as shown in Equation (5).

$$I_z = I_\alpha + I_\beta \cdot i \tag{5}$$

where I_z is the constructed complex signal.

The instantaneous amplitude and instantaneous phase are obtained by calculating the mode and amplitude angle of the constructed analytic signal. The mode and amplitude angles of I_z are obtained as follows:

$$\begin{cases} |I_z| = \sqrt{{I_\alpha}^2 + {I_\beta}^2} = a(t) \\ \arg(I_z) = \tan^{-1}\left(\dfrac{I_\beta}{I_\alpha}\right) = 2\pi f_M t = \varphi(t) \end{cases} \tag{6}$$

where $a(t)$ is the instantaneous amplitude and $\varphi(t)$ is the instantaneous phase.

The instantaneous frequency is the reciprocal of the instantaneous phase, i.e.,

$$f(t) = \frac{1}{2\pi} \cdot \frac{d\varphi(t)}{dt} \tag{7}$$

where $f(t)$ is the instantaneous frequency.

The instantaneous amplitude and instantaneous frequency are the instantaneous information of the multi-sensor information fusion of the three-phase current signal, reflecting the comprehensive characteristics of the three-phase current.

2.3. Calculation of Coefficient of Variation

The coefficient of variation (C.V.) is the ratio of the standard deviation value to the mean value, which reflects the degree of variation of each observation. The coefficient of variation is a dimensionless statistic.

The mean value μ is shown in the following equation.

$$\mu = \frac{\sum_{i=1}^{n} x_i}{n} \tag{8}$$

where x_i is the i-th data and n is the data length.

The sample standard deviation value σ is shown in the following equation.

$$\sigma = \sqrt{\frac{\sum_{i=1}^{n} (x_i - \mu)^2}{n-1}} \tag{9}$$

From the definition of the coefficient of variation, the coefficient of variation c_v is obtained by associating Equations (8) and (9):

$$c_v = \frac{\sigma}{\mu} \tag{10}$$

The coefficient of variation is defined only when the mean is not zero and is usually used when the mean is greater than zero. The coefficient of variation measures the fluctuation of the overall data. By calculating the coefficient of variation of the instantaneous frequency and instantaneous amplitude, the fluctuation status can be analyzed.

Both instantaneous amplitude and instantaneous frequency are basic features of a signal and can be used to analyze the characteristics and variation patterns of a signal. The coefficient of variation of the instantaneous information (instantaneous frequency and instantaneous amplitude) of the motor current, reflecting the instantaneous amplitude and instantaneous frequency fluctuations, can reflect the symmetry of the three-phase current signal during motor operation.

3. Simulation Analysis and Experimental Verification

3.1. Three-Phase Unbalance Simulation and Analysis under Amplitude Deviation and Phase Deviation

In this section, simulation experiments are conducted to adjust the deviations of single-phase amplitude and phase and to analyze and discuss the effects of different amplitude and phase deviations on the three-phase unbalance. The simulated signal is shown in Equation (11). When there is no deviation, the three-phase current amplitude is set to 0.5 A, the signal fundamental frequency is 100 Hz, and the U-phase, V-phase, and W-phase phases are $2\pi/3$, 0, $-2\pi/3$, respectively. The sampling frequency is 20 kHz.

$$\begin{cases} I_u = a \cdot \cos(2\pi f_M t + \theta_u) \\ I_v = a \cdot \cos(2\pi f_M t + \theta_v) \\ I_w = a \cdot \cos(2\pi f_M t + \theta_w) \end{cases} \tag{11}$$

where a is the signal amplitude, f_M is the signal fundamental frequency, θ is the signal phase, I_u, I_v, and I_w are the U-phase, V-phase, and W-phase current signals, respectively, and θ_u, θ_v, and θ_w are the U-phase, V-phase, and W-phase current phases, respectively.

The following subsubsections analyze the amplitude deviation effect and phase deviation effect, respectively.

3.1.1. Effect of Amplitude Deviation

For Equation (11), the U-phase current amplitude a is adjusted from 0.5 A to 1.5 A at 0.1 A intervals, where the U-phase amplitude is 0.9 times and 1.1 times the balanced three-phase current signal, as shown in Figure 2. The instantaneous frequency and instantaneous amplitude, when the U-phase amplitude is 1.1 times the balanced one, are shown in Figure 3. Amplitude deviation affects the transient information performance, i.e., fluctuations in instantaneous frequency and instantaneous amplitude.

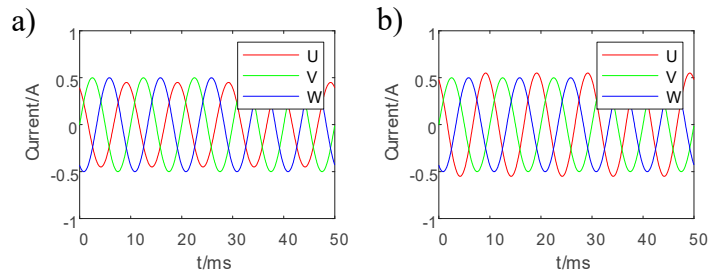

Figure 2. Three-phase current signal with different single-phase amplitude deviation: (**a**) U-phase amplitude is 0.9 times the balanced; (**b**) U-phase amplitude is 1.1 times the balanced.

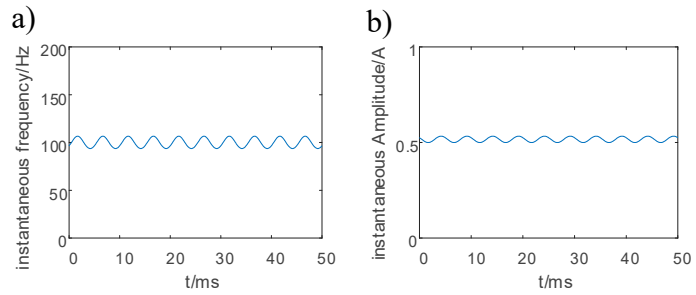

Figure 3. The U-phase amplitude at 1.1 times the balanced: (**a**) instantaneous frequency; and (**b**) instantaneous amplitude.

The U-phase amplitude deviation corresponds to the variation of the instantaneous frequency coefficient of variation and the instantaneous amplitude coefficient of variation of the three-phase currents, as shown in Figure 4. The C.V. of the instantaneous frequency and the C.V. of the instantaneous amplitude increase with an increasing amplitude deviation.

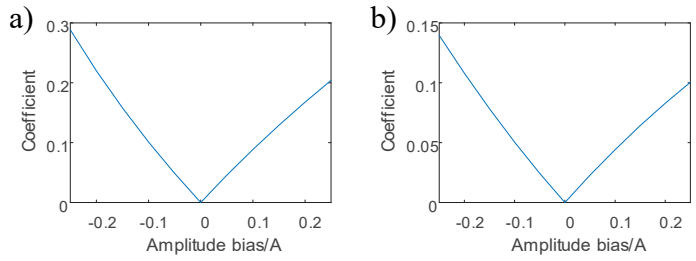

Figure 4. Different amplitude deviations correspond to the following: (**a**) Variation in instantaneous frequency coefficient of variation; (**b**) variation in instantaneous amplitude coefficient of variation.

3.1.2. Effect of Phase Deviation

For Equation (11), the deviation value of the U-phase phase θ_u is adjusted from $-\pi/3$ to $\pi/3$ with an interval of $\pi/15$, where the three-phase current signal is shown in Figure 5 when the U-phase is $\pi/15$ lagged and $\pi/15$ ahead of the balanced. The instantaneous frequency and instantaneous amplitude when the U-phase phase is $\pi/15$ ahead of the relative balance are shown in Figure 6. Phase deviation affects the transient information performance, i.e., fluctuations in instantaneous frequency and instantaneous amplitude.

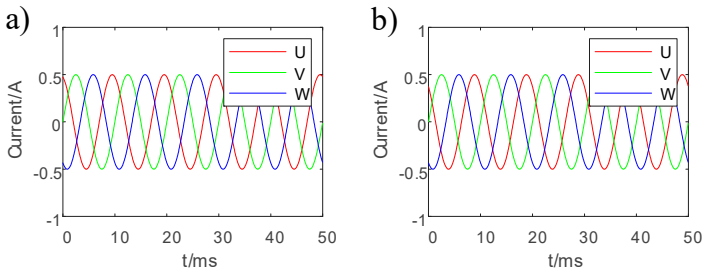

Figure 5. Three-phase current signals with different single-phase phase deviations: (**a**) U-phase is $\pi/15$ lagged after the balanced; (**b**) U-phase is $\pi/15$ ahead of the balanced.

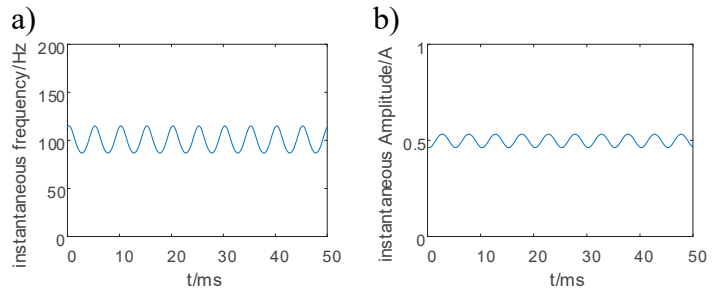

Figure 6. The phase of the U-phase current is $\pi/15$ ahead of the balanced: (**a**) instantaneous frequency; and (**b**) instantaneous amplitude.

The U-phase phase variation corresponds to the variation in the instantaneous frequency coefficient of variation and the instantaneous amplitude coefficient of variation of the three-phase currents, as shown in Figure 7. The C.V. of the instantaneous frequency and the C.V. of the instantaneous amplitude increase with an increasing phase deviation.

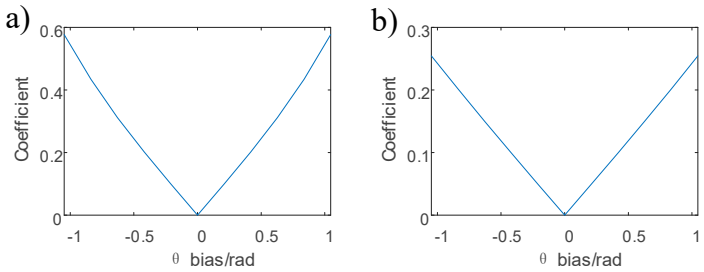

Figure 7. Different phase deviations correspond to the following: (**a**) variation in instantaneous frequency coefficient of variation; (**b**) variation in instantaneous amplitude coefficient of variation.

The deviation of amplitude and phase in the three-phase current affects the instantaneous state. From Figures 4 and 7, it can be seen that for both amplitude deviation and phase deviation, the coefficient of variation increases as the deviation increases. Comparing Figures 4 and 7, it can be seen that both amplitude distortion and phase distortion lead to changes in the instantaneous frequency variation coefficient and instantaneous amplitude variation coefficient, i.e., the instantaneous information variation coefficient increases when the deviation from the three-phase balance state increases. The unbalance of a phase current

affects the time domain characteristics of the instantaneous amplitude and instantaneous frequency extracted from the three-phase current. The proposed method converts the three-phase signal to obtain the instantaneous information characteristics, which can analyze the unbalance situation more comprehensively and intuitively.

The symmetrical components method is used to obtain the three-phase voltage/current vector through FFT, transform the amplitude and phase, and analyze the amplitude of its negative sequence component in the case of amplitude deviation and phase deviation [23]. Since this paper examines the effects of current, the equation can be expressed as Equation (12). For comparison, the coefficient is not multiplied by 100.

$$\mathrm{F} = \frac{I_2}{I_1} \tag{12}$$

where I_1 and I_2 are the positive and negative vector components of the current, respectively.

The results are shown in Figure 8, and it can be seen that the symmetrical components method has the same trend as the method proposed in this paper.

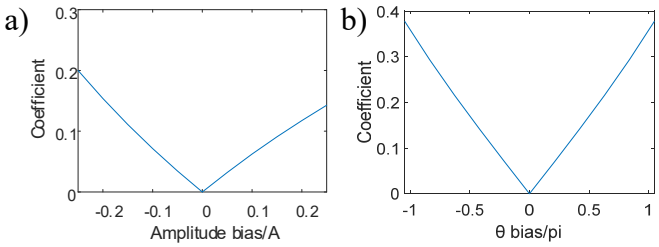

Figure 8. Analysis of symmetrical components method coefficient changes: (**a**) symmetrical components method coefficient changes corresponding to different amplitudes deviations; (**b**) symmetrical components method coefficient changes corresponding to different phase deviations.

Analyzing the main part of the algorithm proposed in this paper, the time complexity of the Park vector demodulation method is $\mathrm{O}(n)$, where n is the data length. For the symmetrical components method, the phase and amplitude of the three-phase current are mainly obtained by FFT. Ignoring the low-order components, the time complexity is approximately $\mathrm{O}(n\log n)$, where n is the data length.

The simulation experiment uses Matlab R2020b, the CPU is Intel Core i5-2400 (3.1 GHz), and the memory is 8 GB (1333 MHz). The number of sampling points is N = 1000, the single calculation time for Park vector demodulation calculation amplitude analysis is 0.344 ± 0.096 ms, and the calculation time of the phase analysis single is 0.235 ± 0.042 ms. The single calculation time of amplitude analysis using the symmetrical components method is 13.407 ± 0.607 ms, and the single calculation time of phase analysis is 12.609 ± 0.294 ms. The calculation time of the main part of the method proposed in this paper is less than that of the symmetrical components method.

3.2. Simulation and Analysis of Three-Phase Unbalance with Continuous Change in Amplitude

This subsection simulates the unbalance of the continuous change in amplitude, and the simulation signal is shown in Equations (13) and (14). The three-phase current amplitude is 0.5 A, the signal fundamental frequency is 50 Hz, the U-phase, V-phase, and W-phase are $2\pi/3$, 0, and $-2\pi/3$, respectively, A_t changes with time linearly from 1.1 to 1.3, and the sampling frequency is 20 kHz.

$$\begin{cases} I_u = a\cdot\cos(2\pi f_M t + \theta_u)\cdot A_t \\ I_v = a\cdot\cos(2\pi f_M t + \theta_v) \\ I_w = a\cdot\cos(2\pi f_M t + \theta_w) \end{cases} \tag{13}$$

$$A_t = g + h\cdot t \tag{14}$$

where a is the signal amplitude, f_M is the signal fundamental frequency, θ is the signal phase, I_u, I_v, and I_w are the U-phase, V-phase, and W-phase current signals, respectively, and θ_u, θ_v, and θ_w are the U-phase, V-phase, and W-phase current phases, respectively; A_t is the amplitude time-varying signal, g is constant, and h is the rate of change.

The three-phase unbalanced current signal with a continuous change in amplitude is slid, and the sliding window sizes are 100 ms and 50 ms, respectively, as shown in Figure 9.

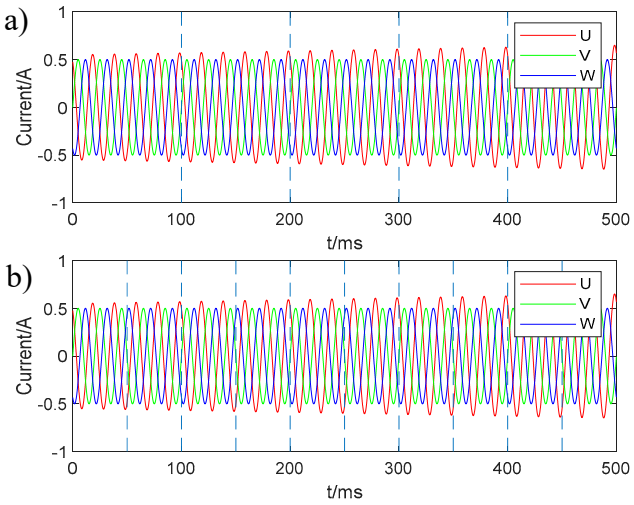

Figure 9. Different sliding window sizes for three-phase unbalanced current signals with continuous changes in amplitude: (**a**) the sliding window size is 100 ms; (**b**) the sliding window size is 50 ms.

The coefficient of variation results for instantaneous frequencies and instantaneous amplitudes under different sliding window sizes are shown in Figures 10 and 11.

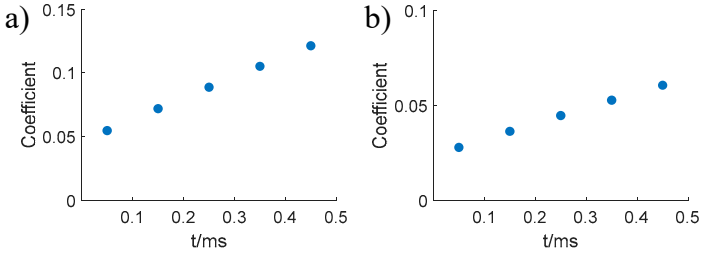

Figure 10. Analysis of three-phase unbalance with continuous amplitude variation using the method of this paper when the sliding window size is 100 ms: (**a**) the C.V. of the instantaneous frequency; and (**b**) the C.V. of the instantaneous amplitude.

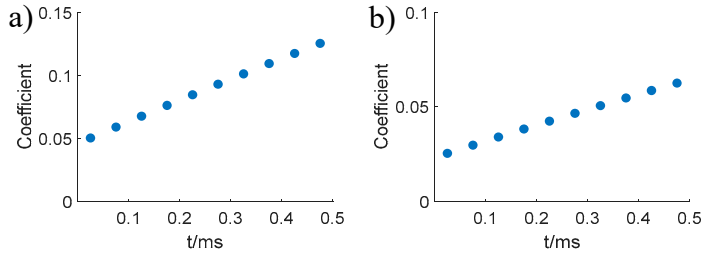

Figure 11. Analysis of three-phase unbalance with continuous amplitude variation using the method of this paper when the sliding window size is 50 ms: (**a**) the C.V. of the instantaneous frequency; and (**b**) the C.V. of the instantaneous amplitude.

As can be seen from Figures 10 and 11, for the unbalanced signal with a continuous change in amplitude, the coefficient of variation value of the instantaneous information

increases as the unbalance increases. When reducing the sliding window size, the proposed method can still characterize the change in the unbalance. For the symmetrical components method, three-phase unbalance is analyzed as shown in Figure 12a. The results are not accurate when the sliding window size is smaller, as shown in Figure 12b. In addition, the frequency resolution of FFT will be affected by the number of sampling points.

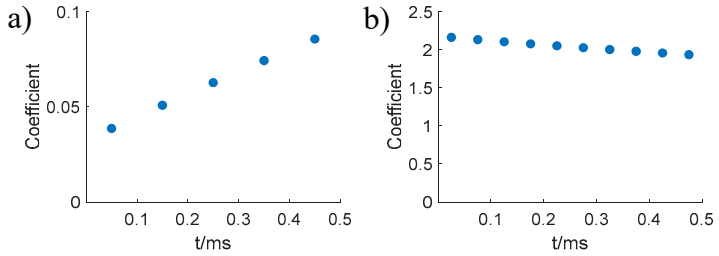

Figure 12. Analysis of three-phase unbalances with continuous amplitude variation using the symmetrical components method when the sliding window size is as follows: (**a**) 100 ms; (**b**) 50 ms.

For a better test of the effect of the sliding window size (the number of sampling points) on the analysis of three-phase unbalance and the analysis of the effect of integral period sampling, the starting points of the U, V, and W phase current signals (t = 0) were selected and fixed, with data of different lengths, and the FFT was calculated to obtain the phase at the maximum amplitude (fundamental frequency), with the results shown in Figure 13. Since the original simulated signal used in this section is in sine form and the FFT calculation using Matlab gives the cosine form with a difference of 90°, the phase calculated by the FFT is obtained by subtracting 90° from the phase of the original signal.

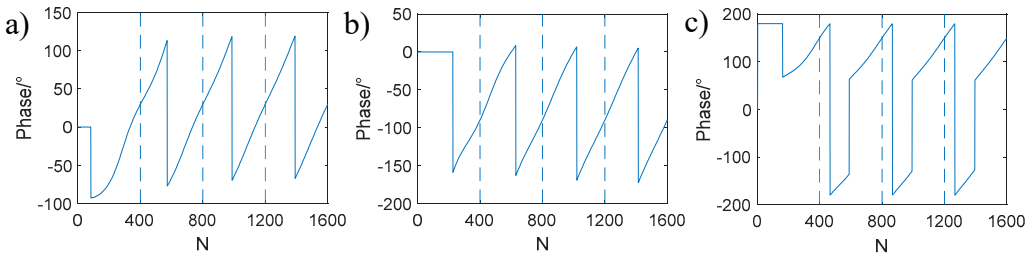

Figure 13. The phase corresponding to the fundamental frequency is obtained using FFT for different data points: (**a**) U-phase, (**b**) V-phase, (**c**) W-phase.

The signal integral period T_1 = 20 ms and its multiples T_n (i.e., when the data point is 400 and its multiples), where n is the number of multipliers, as marked by the dashed line in Figure 13. The results of the 20 ms sliding window are shown in Figure 14, where both the proposed method and the symmetric component method can reflect the change in three-phase unbalance. The results of the 10 ms sliding window are shown in Figure 15, where the length of the sliding window is less than the integral period T_1, and the FFT calculation results required by the symmetrical components method have spectral leakage, and the amplitude and frequency obtained are inaccurate, making the results of the symmetrical components method inaccurate. Similarly, as shown in Figure 12b, the 50 ms sliding window (2.5 times T_1) is not a multiple of the integral period of the signal, and there is a difference between the calculated phase and the phase calculated at the integral period, so the results of the symmetrical components method cannot truly reflect the change in the three-phase unbalance. For the method proposed in this paper, the change in three-phase unbalance can still be reflected under the sliding window of 10 ms.

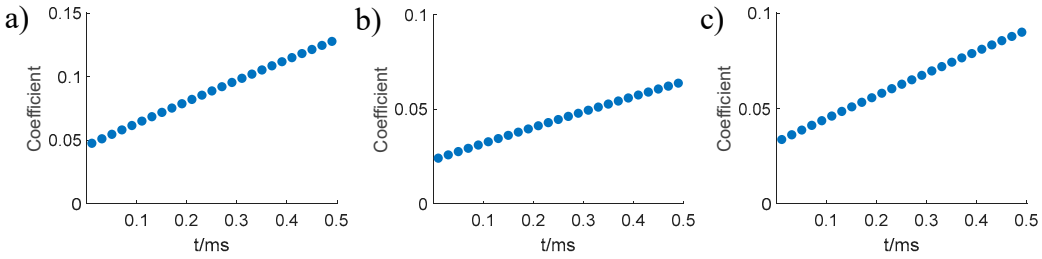

Figure 14. The sliding window is 0.02 s: (**a**) the C.V. of the instantaneous frequency; (**b**) the C.V. of the instantaneous amplitude; (**c**) the symmetrical components method.

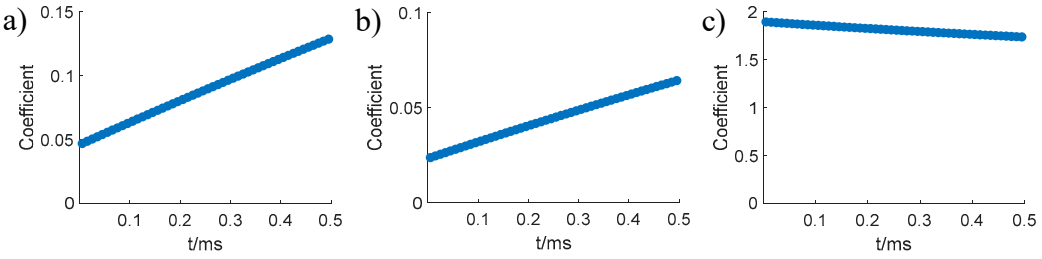

Figure 15. The sliding window is 0.01 s: (**a**) the C.V. of the instantaneous frequency; (**b**) the C.V. of the instantaneous amplitude; (**c**) the symmetrical components method.

For the choice of window width, it can be no less than the integral period, i.e., the inverse of the instantaneous frequency of the signal. The method proposed in this paper does not require the window length to be chosen as a multiple of the integral period and has better window length adaptability. In summary, compared with the symmetrical components method, the proposed method can still analyze the three-phase unbalance with fewer data points (smaller sliding window size).

The switching frequency of the converter generates noise [24,25]. Based on Equations (13) and (14), the analysis of the effect of switching noise is simplified by using the switching frequency superimposed on random noise, as shown in the following equation. The high-frequency signal amplitude is set to 0.02 times the fundamental frequency signal amplitude, the switching frequency is 1 kHz, the initial phase is 0 rad, and the random noise amplitude is 0.01 times the fundamental frequency signal amplitude.

$$\begin{cases} I_u = a\cdot\cos(2\pi f_M t + \theta_u)\cdot A_t + b\cdot\cos(2\pi f_N t + \theta_{uN}) + c\cdot noise_u \\ I_v = a\cdot\cos(2\pi f_M t + \theta_v) + b\cdot\cos(2\pi f_N t + \theta_{vN}) + c\cdot noise_v \\ I_w = a\cdot\cos(2\pi f_M t + \theta_w) + b\cdot\cos(2\pi f_N t + \theta_{wN}) + c\cdot noise_w \end{cases} \quad (15)$$

where b is the high-frequency signal amplitude, f_N is the switching frequency, θ_{uN}, θ_{vN}, and θ_{wN} are the switching frequency phases, c is the random noise amplitude, and $noise_u$, $noise_v$, and $noise_w$ are the random noise.

The simulation signal is shown in Figure 16, with the sliding window set to 50 ms.

The FFT values and the total harmonic distortion (THD) of the U, V, and W phase current signals are calculated separately, and the results are shown in Figure 17 (the fundamental frequency amplitude is 100%). For three-phase current signals, high-frequency signals can be seen on the spectrum, as well as many noise frequencies. For U-phase currents, many side frequencies are present near the fundamental frequency on the spectrum.

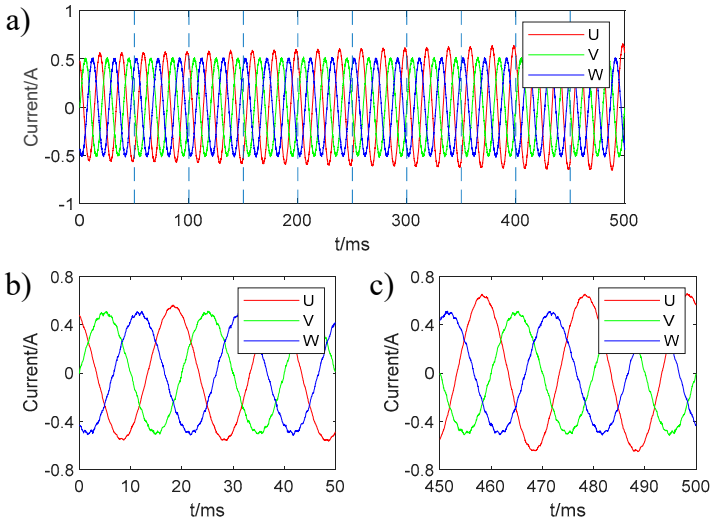

Figure 16. Three-phase unbalanced current signals with continuous changes in amplitude after adding switching noise: (**a**) 0 to 500 ms signal, (**b**) 0 to 50 ms signal, (**c**) 450 ms to 500 ms signal.

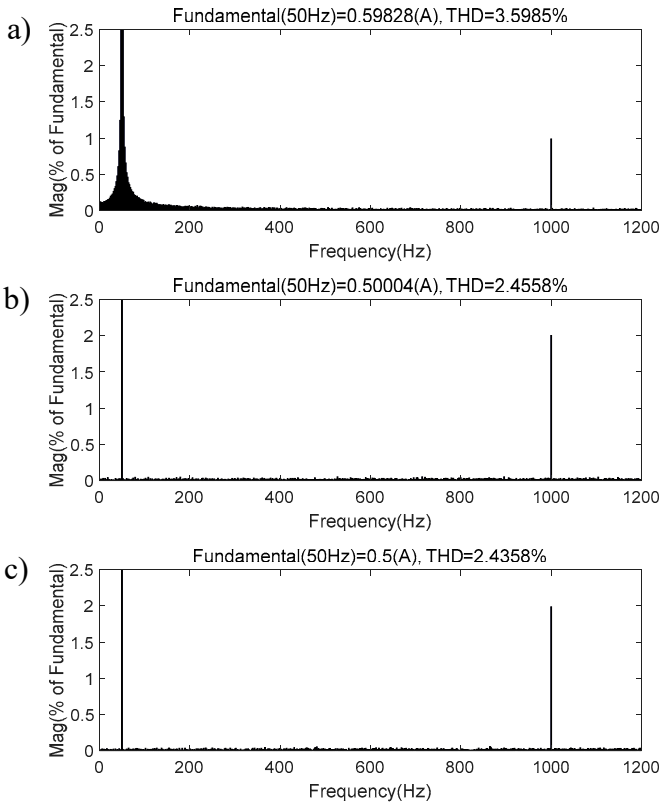

Figure 17. The FFT results and the THD of the current signals of phases U, V, and W: (**a**) U-phase; (**b**) V-phase; (**c**) W-phase.

The analysis results of the proposed method are shown in the Figure 18.

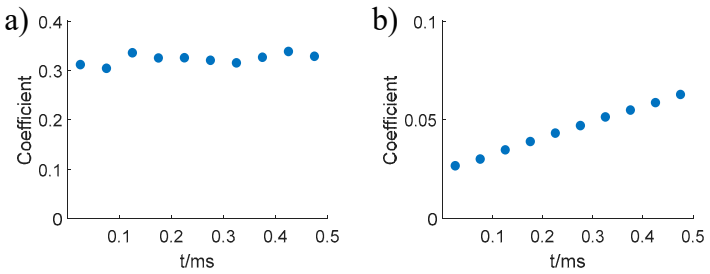

Figure 18. When adding switching noise: (**a**) the C.V. of the instantaneous frequency; (**b**) the C.V. of the instantaneous amplitude.

From the analysis of the above results, and comparing the results without the addition of switching noise, it can be seen that after the addition of switching noise, the instantaneous frequency results are affected and the instantaneous frequency coefficient of variation can hardly reflect the three-phase unbalance change, while the instantaneous amplitude coefficient of variation can still reflect the unbalance change trend.

3.3. Simulink Simulation and Result Analysis

Using Simulink's "sps_lib" library, a simulation model is constructed to simulate a three-phase unbalance by adjusting the resistance of a varistor, as shown in Figure 19 (phases A, B, and C, equivalent to phases U, V, and W). The three-phase programmable voltage source has an RMS value of 380 V, a phase of 0°, and a frequency of 60 Hz. The three-phase asynchronous motor (squirrel cage) has an output power of 18.5 kW, an RMS value of 380 V, a frequency of 60 Hz, and pole pairs of 2. The motor stator resistance and inductance are 0.597 Ω and 0.001 H, respectively, the rotor resistance and inductance are 0.626 Ω and 0.005 H, respectively, and the mutual inductance is 0.035 H. Resistors R1 and R2 are 0.002 Ω, R3 is 0.001 Ω, and R4 is 10-kΩ. Breaker 1 and Breaker 2 have an interconnection resistance of 0.001 Ω. Breaker 1 is on from 0 s to 2π seconds and 4π seconds to the stop time and off the rest of the time; breaker 2 is on from 2π seconds to 4π seconds and off the rest of the time. A sinusoidal signal of amplitude 1, phase of 0 rad, and frequency of 0.5 rad/s with an instantaneous negative amplitude is set as the value of the variable resistor. The stop time (duration of the simulation) is 16 s.

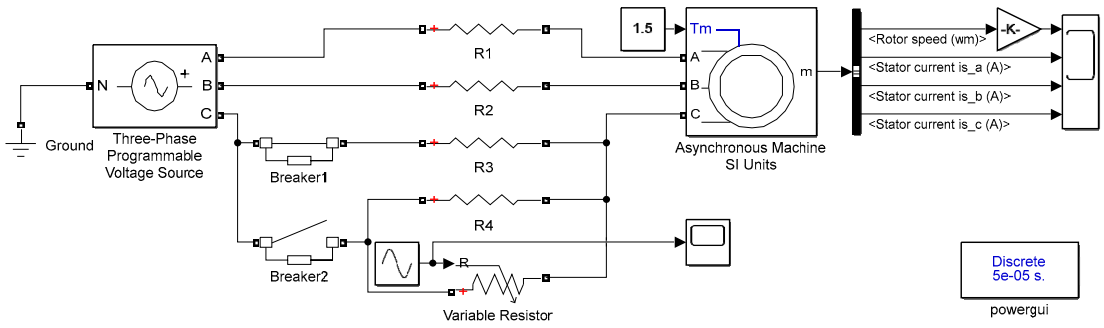

Figure 19. Simulation of three-phase unbalance by adjusting the resistance of the varistor.

Simulation result data, such as stator currents, were recorded and the three-phase current signals between 3 and 15 s are shown in Figure 20. Using the method proposed in this paper to calculate the three-phase current instantaneous information with a sliding window of 0.5 s, the results are shown in Figure 21.

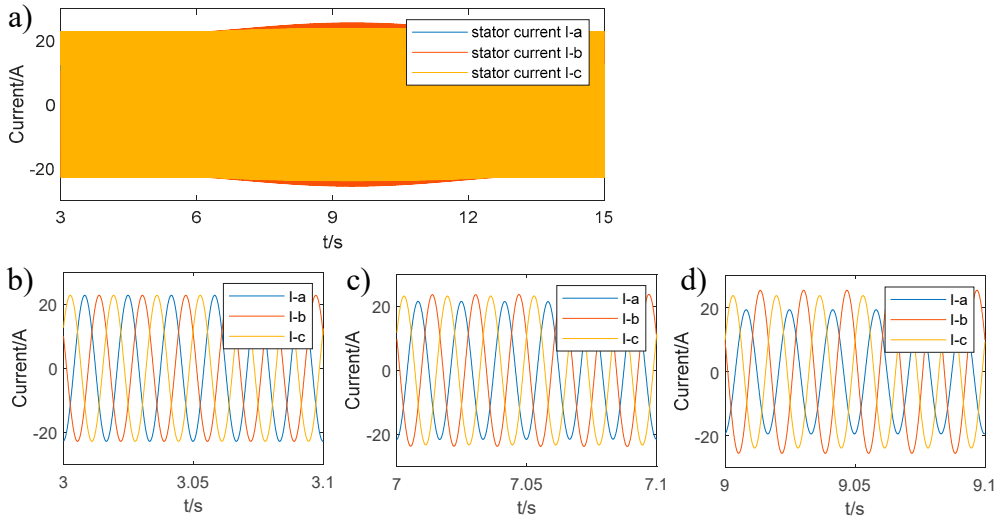

Figure 20. Adjusting the variable resistor, the three-phase unbalance amplitude changes: (**a**) 3–15 s signal; (**b**) 3–3.1 s signal; (**c**) 7–7.1 s signal; (**d**) 9–9.1 s signal.

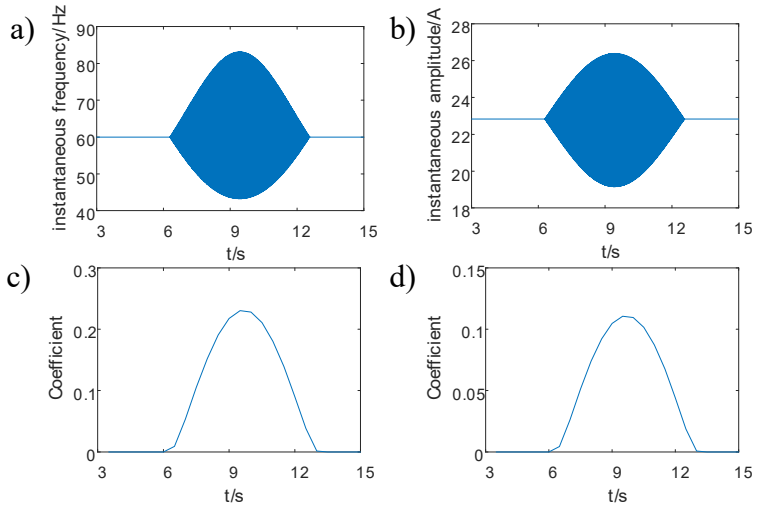

Figure 21. Results of instantaneous information with a sliding window of 0.5 s: (**a**) instantaneous frequency; (**b**) instantaneous amplitude; (**c**) the C.V. of the instantaneous frequency; (**d**) the C.V. of the instantaneous amplitude.

For three-phase unbalance cases with continuously varying amplitudes, the proposed method can effectively represent the degree of three-phase unbalance variation.

Usually in practical application scenarios, disturbances, such as harmonics, may be involved in the power supply. The 5th and 8th harmonics are added to the voltage source, and the harmonics are superimposed on the fundamental signal from a 0.05 s duration to the stop time. The 5th harmonic is set to a negative sequence with an amplitude of 0.03 of the amplitude of the main positive sequence component (fundamental frequency voltage) and a phase of 0°. The 8th harmonic is set to a negative sequence with an amplitude of 0.01 of the amplitude of the main positive sequence component (fundamental frequency voltage) and a phase of 0°. The three-phase current signal is shown in Figure 22. As can be seen in Figure 22b, after superimposing the harmonics, it can be seen by comparing Figure 20b that the three-phase current signal is distorted.

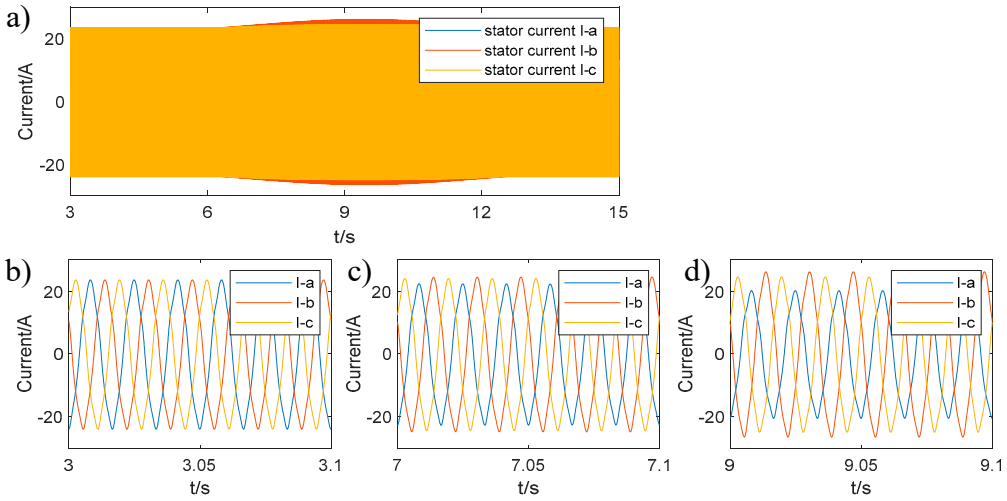

Figure 22. After superimposing harmonics, the variable resistor corresponding to the change in amplitude of the three-phase unbalance is adjusted: (**a**) 3 s–15 s signal; (**b**) 3 s–3.1 s signal; (**c**) 7 s–7.1 s signal; (**d**) 9 s–9.1 s signal.

The FFT values and the THD of the 3–4 s signals of phases A, B, and C were calculated separately, and the results are shown in Figure 23 (the fundamental frequency amplitude is 100%). After superimposing the harmonics, the 5th and 8th harmonics can be seen in the FFT spectrum, both with a THD of 4.0921%.

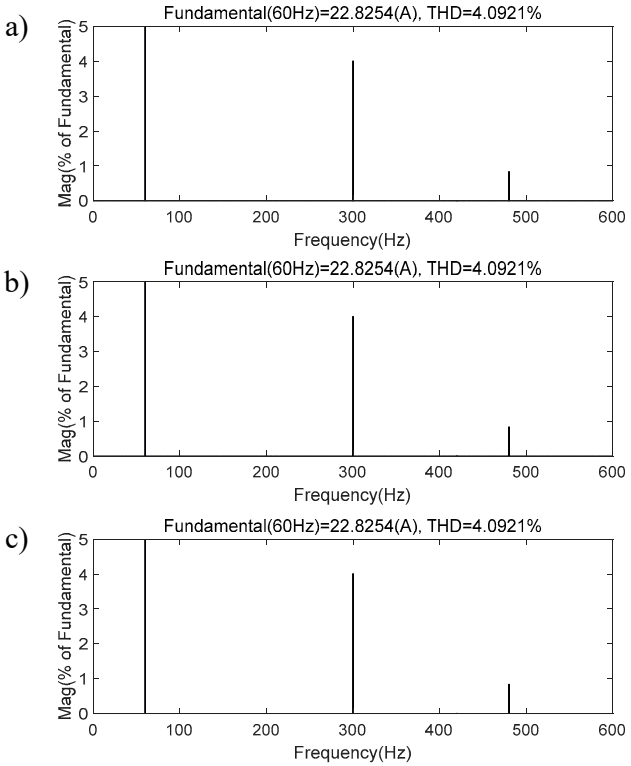

Figure 23. The FFT results and the THD of the 3 s–4 s current signals of phases A, B, and C: (**a**) A-phase; (**b**) B-phase; (**c**) C-phase.

After superimposing the harmonics, the three-phase current instantaneous information was calculated using the method proposed in this paper with a sliding window of 0.5 s, and the results are shown in Figure 24.

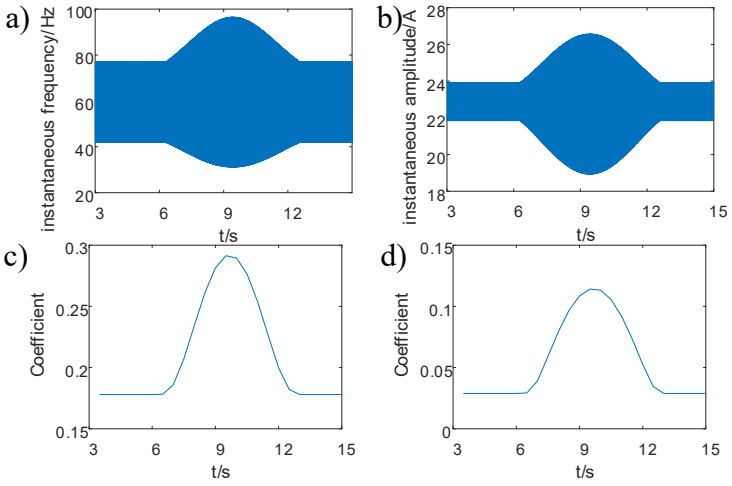

Figure 24. Results of instantaneous information after superimposing harmonics with a sliding window of 0.5 s: (**a**) instantaneous frequency; (**b**) instantaneous amplitude; (**c**) the C.V. of the instantaneous frequency; (**d**) the C.V. of the instantaneous amplitude.

Comparing the instantaneous frequency and amplitude when the resistance of the variable resistor is not adjusted shows that the calculated instantaneous frequency and amplitude of the current signal fluctuate after the superimposition of harmonics and that the coefficient of variation of the instantaneous frequency and the coefficient of variation of the instantaneous amplitude increase compared to the results when there are no harmonics. The coefficient of variation of the instantaneous frequency and amplitude varies with the resistance value during the adjustment of the variable resistor. The superimposed harmonics cause signal distortion, resulting in fluctuations in the instantaneous frequency and instantaneous amplitude.

The total harmonic distortion can reflect the non-sinusoidal waveform state and analyze the degree of harmonic pollution. The transient information changes caused by harmonics can be considered for analysis as a power quality state. Even if harmonics are superimposed, the proposed method can still reflect the change in the unbalance trend for three-phase unbalance caused by changes in amplitude.

3.4. Experimental Validation and Analysis

The main components of this section of the test bench are shown in Figure 25, which are mainly composed of an inverter, motor, phase controller, gearbox, magnetic powder clutch, and other components, of which the motor is replaceable. The current sensor was clamped to the motor power input, model Fluke i200 s, 100 mV/A range. The sensor data were collected using a NI-USB 9234 data acquisition card. The sampling frequency was 3200 Hz. The speed (rotational frequency) settings were 5 Hz, 10 Hz, 15 Hz, and 20 Hz. The fault motor is a motor with voltage unbalance and a single phase (abbreviated as MVUSP).

Adjustment of the motor current three-phase unbalance is achieved by rotating the phase controller knob, gradually adjusting it up from small, then adjusting it down, and then repeating it once. The motor runs at 5 Hz, 10 Hz, 15 Hz, and 20 Hz, and the three-phase current signal obtained by adjusting the three-phase unbalance through the knob is shown in Figure 26. When the knob is rotated clockwise, the W-phase current amplitude decreases and the three-phase unbalance increases; when the knob is rotated counterclockwise, the W-phase current amplitude increases and the three-phase unbalance decreases.

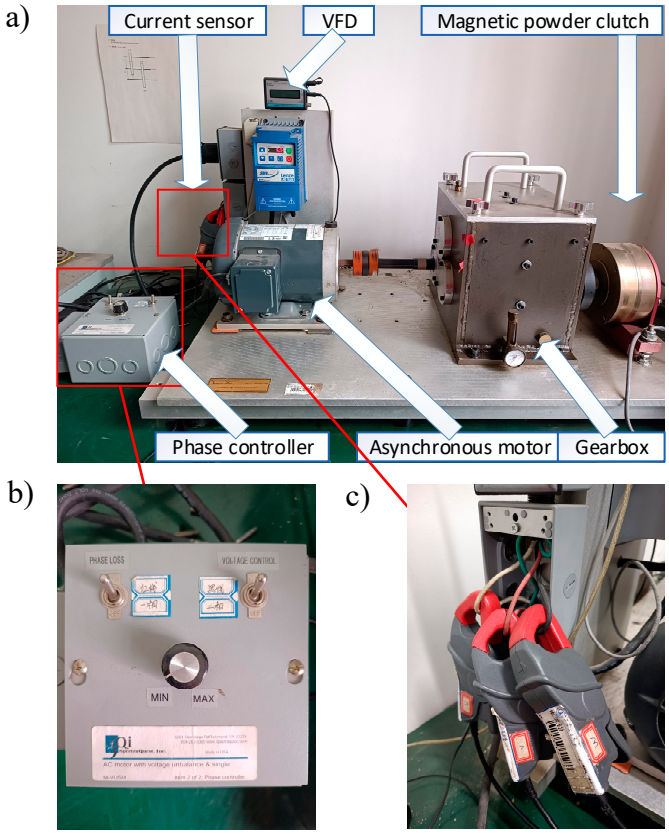

Figure 25. Gearbox dynamics test bench: (**a**) composition of the experimental bench; (**b**) phase controller; (**c**) current sensor clamping.

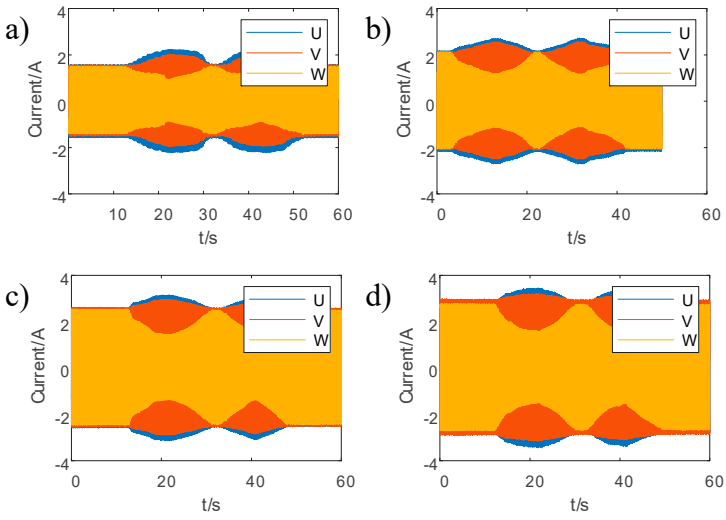

Figure 26. Three-phase current signal to adjust the degree of three-phase unbalance at different rotational frequencies: (**a**) 5 Hz; (**b**) 10 Hz; (**c**) 15 Hz; (**d**) 20 Hz.

The segmented signals in different periods (0–1 s, 15–16 s, 21–22 s) at a 15 Hz rotational frequency are shown in Figure 27.

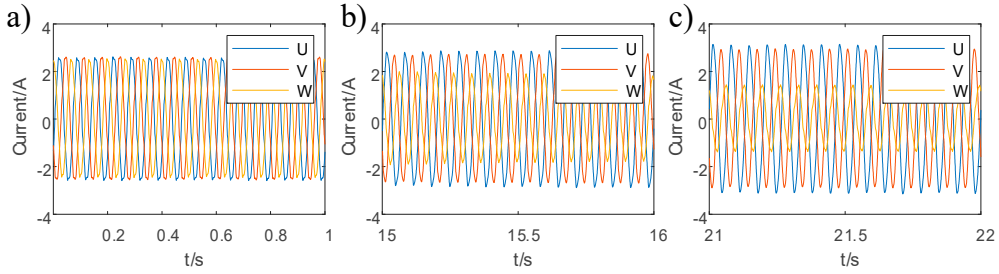

Figure 27. Three-phase current at 15 Hz rotational frequency of different periods: (**a**) 0–1 s; (**b**) 15–16 s; (**c**) 21–22 s.

The sliding window size is 1 s. The instantaneous frequency and instantaneous amplitude at 15 Hz are shown in Figure 28. The results of the C.V. of the instantaneous information are shown in Figure 29. The results of the symmetrical components method are shown in Figure 30. Comparing Figures 29 and 30, it can be seen that the C.V. of the instantaneous frequency and the C.V. of the instantaneous amplitude have the same trend as the three-phase unbalance results calculated using the symmetrical components method as the 1 s sliding window.

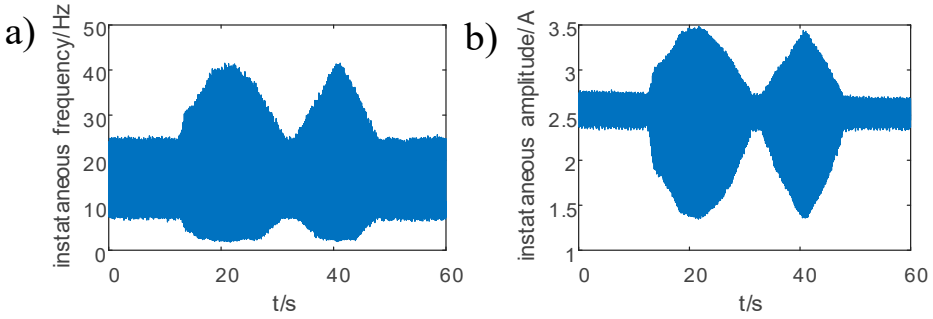

Figure 28. Instantaneous information at a 15 Hz rotational frequency: (**a**) instantaneous frequency; (**b**) instantaneous amplitude.

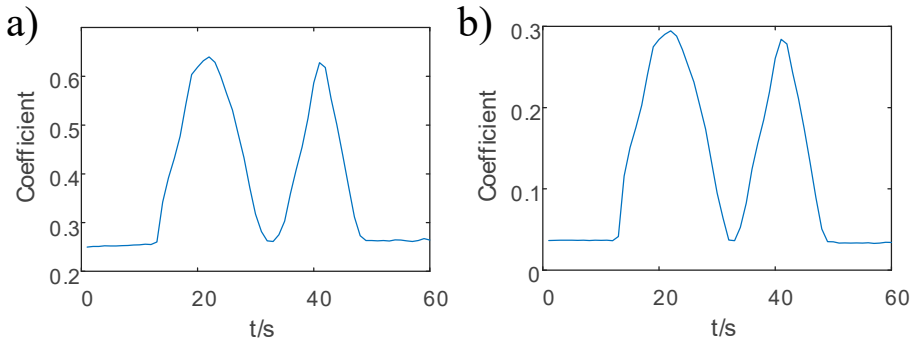

Figure 29. The results of the proposed method at a 15 Hz rotational frequency: (**a**) the C.V. of the instantaneous frequency; (**b**) the C.V. of the instantaneous amplitude.

The C.V. of the instantaneous frequency and the C.V. of the instantaneous amplitude were calculated for the three-phase unbalanced signals at 5 Hz, 10 Hz, and 20 Hz rotational frequencies, respectively, with a sliding window size of 1 s. The results are shown in Figure 31. Comparing the C.V. of the instantaneous frequency, the C.V. of the instantaneous amplitude, and symmetrical components method coefficients at the same rotational frequency, it can be seen that they have similar trends and are consistent with the results at a 15 Hz rotational frequency. The above results show that both the proposed method and the symmetrical components method can reflect the change in the three-phase unbalance.

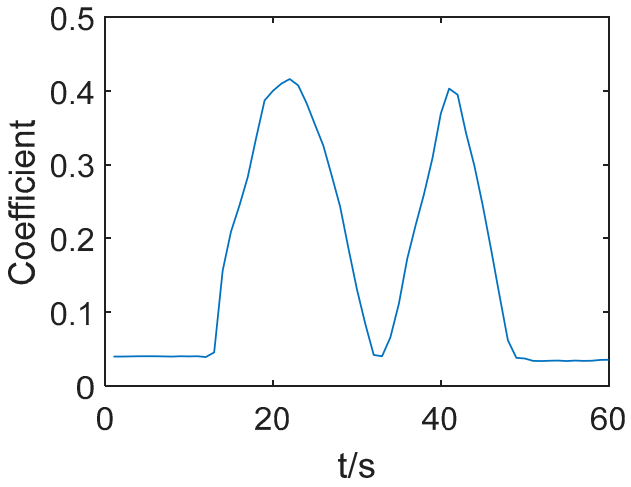

Figure 30. The results of the symmetrical components method at a 15 Hz rotational frequency.

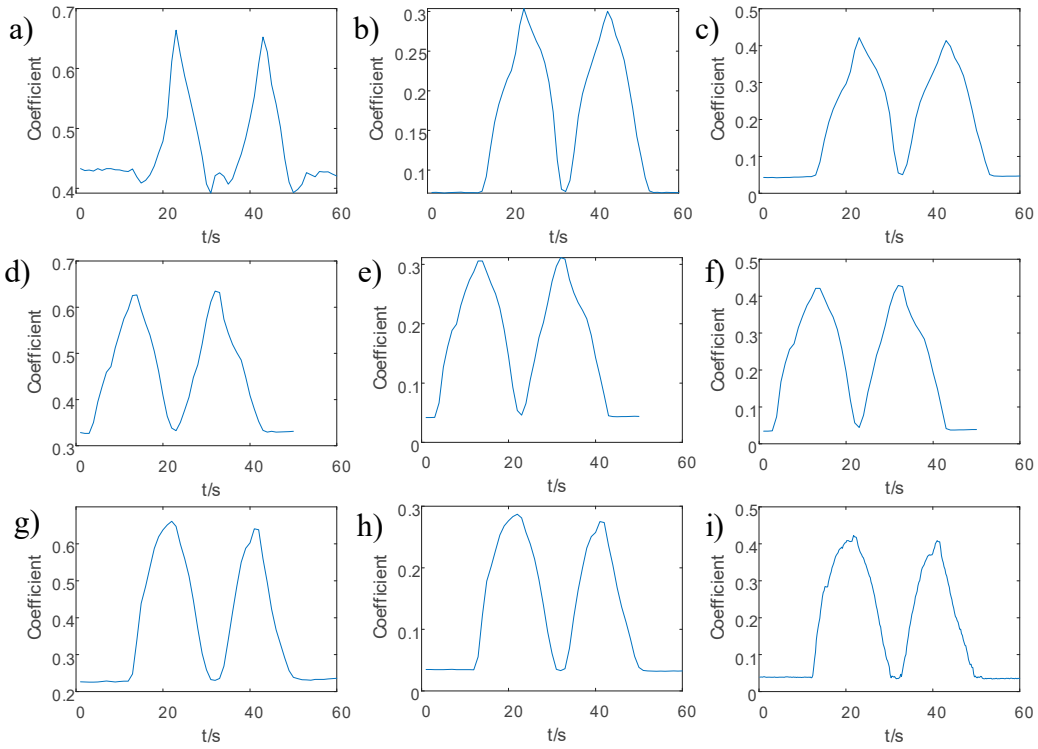

Figure 31. Adjustment of three-phase unbalance at different rotational frequencies, with the results of this paper's method and symmetrical components method (the C.V. of the instantaneous frequency, the C.V. of the instantaneous amplitude, and the symmetrical components method), while the sliding window size is 1 s: (**a**–**c**) 5 Hz; (**d**–**f**); 10 Hz; (**g**–**i**) 20 Hz.

The effects of different sliding window lengths on the method proposed in this paper and the symmetrical components method are analyzed as follows. For the three-phase unbalanced signal at a 15 Hz rotational frequency, its single-phase signal period is 1/15 s (about 0.067 s). Considering the sampling frequency at the same time, the sliding window size is set to 0.2 s, 0.1 s, 0.05 s, and 0.02 s, respectively, and the results are shown in Figure 32. By analyzing Figures 29, 30 and 32a–c, it can be seen that the results of the 0.2 s sliding window are similar to those of the 1 s sliding window. As the sliding window size decreases, the instantaneous frequency coefficient of variation and instantaneous amplitude coefficient of variation can still reflect the three-phase unbalance change well when the sliding window size is 0.1 s, but the symmetrical components method has been unable to correctly reflect the

three-phase unbalance change. When the sliding window is 0.05 s and 0.02 s, although the C.V. of the instantaneous frequency and the C.V. of the instantaneous amplitude fluctuate more, the trend of three-phase unbalances can still be seen. The accuracy of the fast Fourier (FFT) calculation results for single-phase currents in the symmetrical components method is affected when the sliding window size is too small. That is, the solved amplitude and phase have large errors, and the positive-sequence, negative-sequence, and zero-sequence are inaccurate, thus affecting the final results. From the above analysis, it can be seen that when the sliding window size is small, the proposed method in this paper can still reflect the change in the three-phase unbalances better than the symmetrical components method. However, when the sliding window size is too small, the deviation of the result of the C.V. of the instantaneous information value increases and affects the analysis.

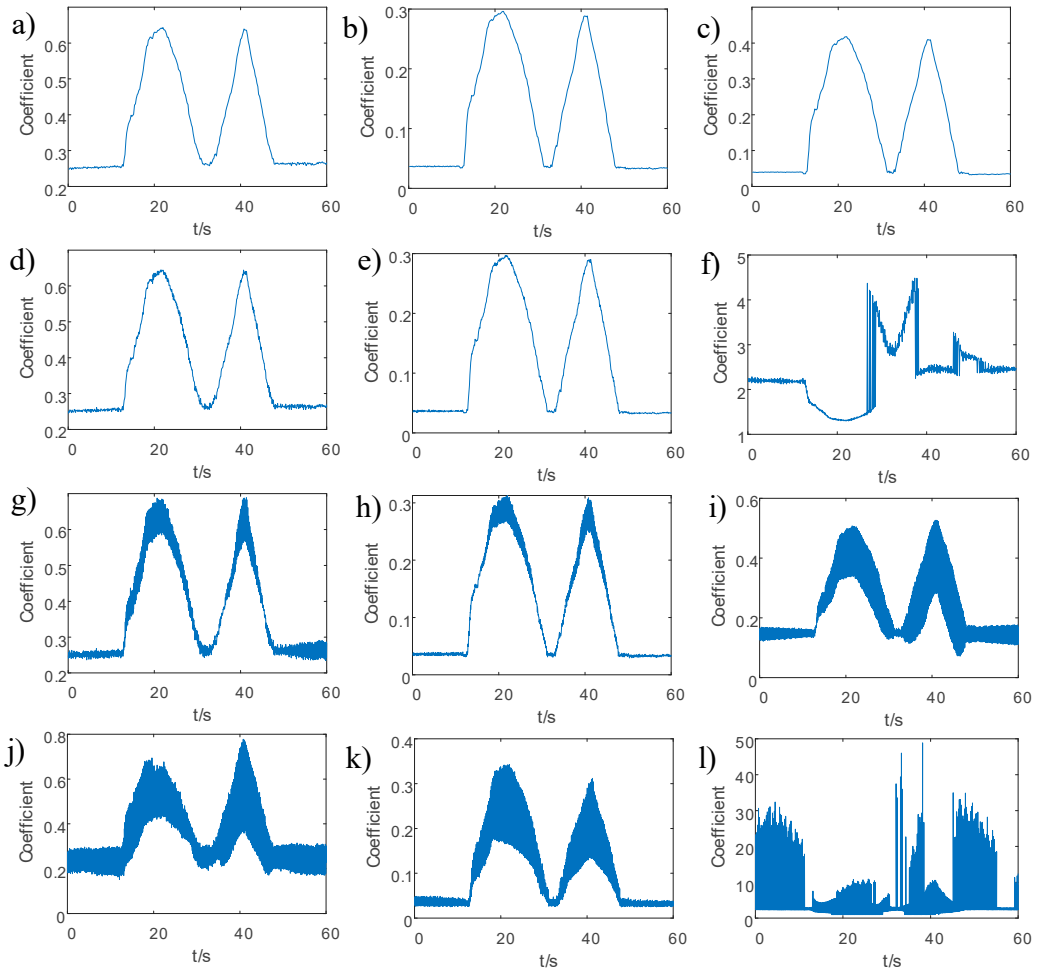

Figure 32. Analysis of different sliding window sizes at a 15 Hz rotational frequency, the results of this paper's method and symmetrical components method (the C.V. of the instantaneous frequency, the C.V. of the instantaneous amplitude, and the symmetrical components method): (**a**–**c**) 0.2 s sliding window; (**d**–**f**) 0.1 s sliding window; (**g**–**i**) 0.05 s sliding window; (**j**–**l**) 0.02 s sliding window.

The mean value of the instantaneous frequency obtained using the proposed method in this paper can be used as a reference for selecting the appropriate sliding window. When the size of the sliding window is too small (less than the reciprocal of the mean value of the instantaneous frequency), the degree of fluctuation of the obtained coefficients increases.

The single sliding window calculation times at different rotational frequencies are analyzed for sliding window sizes of 1 s and 0.2 s, respectively. The calculation is carried out using Matlab R2021b. The CPU used is an Intel Core i7 12700H (base speed 2.3 GHz), and the memory is DDR5 16 GB (4800 MHz). The test was repeated five times, and the mean

value of the test results was counted, as shown in Table 1. For a 1 s sliding window, the calculation time of the proposed method in this paper is 0.022 ± 0.004 times the symmetrical components method, and for a 0.1 s sliding window, the calculation time of the proposed method in this paper is 0.036 ± 0.002 times the symmetrical components method. The computation time of the proposed method in this paper is less than that of the symmetrical components method, i.e., the computation is faster.

Table 1. The single sliding window calculation time at different rotational frequencies.

	1 s Sliding Window		0.2 s Sliding Window	
	The Proposed Method in This Paper (s)	**The Symmetrical Components Method (s)**	**The Proposed Method in This Paper (s)**	**The Symmetrical Components Method (s)**
5 Hz	0.000238	0.010089	0.000078	0.002203
10 Hz	0.000175	0.010281	0.000079	0.002151
15 Hz	0.000218	0.010082	0.000084	0.002157
20 Hz	0.000276	0.010133	0.000072	0.002143

In summary, it can be seen that the three-phase unbalance analysis method based on the instantaneous amplitude coefficient of variation and instantaneous frequency coefficient of variation of three-phase currents requires a smaller sliding window size and faster calculation speed compared to the symmetrical components method. If the sliding window is too small, the results of the proposed method will fluctuate, resulting in an inaccurate analysis, and the appropriate sliding window (greater than the reciprocal of the mean value of the instantaneous frequency) can be selected based on the mean value of the instantaneous frequency.

4. Conclusions

This paper proposes a three-phase unbalanced analysis method based on the instantaneous information of the motor current. The basic process is as follows: obtain the three-phase current signal, construct the phase shift signal via vector demodulation to obtain the instantaneous frequency and instantaneous amplitude of the current signal, calculate its coefficient of variation, and compare and analyze the performance of instantaneous information characteristic coefficients under the three-phase unbalance condition.

Simulation experiments are conducted to analyze the effects of amplitude deviation and phase deviation on the variation coefficients of the instantaneous frequency and instantaneous amplitude, respectively. The continuous change in a three-phase unbalance amplitude is simulated, and its instantaneous performance is analyzed. Compared with the symmetrical components method, the proposed method can still analyze the three-phase unbalance with a smaller sliding window size. Simulation results show that switching noise will affect the C.V. of the instantaneous frequency, while the C.V. of the instantaneous amplitude can still reflect the unbalance change trend. When harmonics are superimposed, the proposed method can still reflect the change in the unbalance trend for three-phase unbalance caused by changes in amplitude.

The experimental verification analyzes the instantaneous frequency and instantaneous amplitude coefficient of variation characteristics when comparing and analyzing the continuous change of the three-phase unbalance of the motor at different speeds. Simulations and experiments show that the proposed method in this paper can analyze motor three-phase unbalance faults.

Advantages: The instantaneous information of the three-phase current is obtained through Park vector demodulation, the calculation result is similar to the trend of the symmetrical components method, the time complexity of this method is smaller than that of the symmetrical components method, and a smaller sliding window is required.

Author Contributions: Conceptualization, X.Z.; Methodology, X.Z. and G.X.; Software, X.Z.; Validation, X.Z. and S.C.; Formal analysis, X.Z. and R.C.; Investigation, X.Z. and X.C.; Resources, X.Z. and G.X.; Data curation, X.Z.; Writing—original draft preparation, X.Z.; Writing—review and editing, X.Z., G.X., X.C., R.C., S.C. and S.Z.; Visualization, X.Z.; Supervision, G.X. and S.Z.; Project administration, G.X.; Funding acquisition, G.X. All authors have read and agreed to the published version of the manuscript.

Funding: This research was supported by the Key Projects in Shaanxi Province (Grant No. 2021GXLH-Z-008), the Science and Technology Plan Project of Xi'an (Grant No. 20KYPT0001-10), and the National Key Research and Development Program of China (Grant No. 2019YFB2004400).

Institutional Review Board Statement: The study did not require ethical approval.

Informed Consent Statement: Not applicable.

Data Availability Statement: Data sharing is not applicable to this article.

Conflicts of Interest: The authors declare no conflict of interest.

References

1. Glowacz, A.; Glowacz, W.; Kozik, J.; Piech, K.; Gutten, M.; Caesarendra, W.; Liu, H.; Brumercik, F.; Irfan, M.; Khan, Z.F. Detection of deterioration of three-phase induction motor using vibration signals. *Meas. Sci. Rev.* **2019**, *19*, 241–249. [CrossRef]
2. Çalış, H. Vibration and motor current analysis of induction motors to diagnose mechanical faults. *J. Meas. Eng.* **2014**, *2*, 190–198.
3. Zarei, J.; Poshtan, J. Bearing fault detection using wavelet packet transform of induction motor stator current. *Tribol. Int.* **2007**, *40*, 763–769. [CrossRef]
4. Thomson, W.T.; Fenger, M. Current signature analysis to detect induction motor faults. *IEEE Ind. Appl. Mag.* **2001**, *7*, 26–34. [CrossRef]
5. Kryter, R.; Haynes, H. *Condition Monitoring of Machinery Using Motor Current Signature Analysis*; Oak Ridge National Lab.: Oak Ridge, TN, USA, 1989.
6. Kapoor, S.R.; Vashishtha, A.; Jethoo, Y.S. Performance analysis of wavelet based techniques for electrical faults signature extraction for squirrel cage induction motor. In Proceedings of the 2014 International Conference on Signal Propagation and Computer Technology (ICSPCT 2014), Ajmer, India, 12–13 July 2014; pp. 71–76.
7. Pineda-Sanchez, M.; Riera-Guasp, M.; Perez-Cruz, J.; Puche-Panadero, R. Transient motor current signature analysis via modulus of the continuous complex wavelet: A pattern approach. *Energy Convers. Manag.* **2013**, *73*, 26–36. [CrossRef]
8. Nordin, N.; Singh, H. Detection and classification of induction motor faults using Motor Current Signature Analysis and Multilayer Perceptron. In Proceedings of the Power Engineering and Optimization Conference (PEOCO), Langkawi, Malaysia, 24–25 March 2014; pp. 35–40.
9. Liang, L.; Xu, G.; Liu, D.; Li, M. A feature extraction method of rotor faults of induction motor based on continuous wavelet transform and singular value decomposition. *Proc. Chin. Soc. Electr. Eng.* **2005**, *25*, 111.
10. Jigyasu, R.; Sharma, A.; Mathew, L.; Chatterji, S. A review of condition monitoring and fault diagnosis methods for induction motor. In Proceedings of the 2018 Second International Conference on Intelligent Computing and Control Systems (ICICCS), Madurai, India, 14–15 June 2018; pp. 1713–1721.
11. Chauhan, A.; Thakur, P.; Raveendhra, D. Assessment of induction motor performance under supply voltage unbalance: A review. In Proceedings of the 2013 Students Conference on Engineering and Systems (SCES), Allahabad, India, 12–14 April 2013; pp. 1–6.
12. Bruzzese, C.; Honorati, O.; Santini, E. Spectral analyses of directly measured stator and rotor currents for induction motor bar breakages characterization by MCSA. In Proceedings of the International Symposium on Power Electronics, Electrical Drives, Automation and Motion, 2006 (SPEEDAM 2006), Taormina, Italy, 23–26 May 2006; pp. 147–152.
13. Sharifi, R.; Ebrahimi, M. Detection of stator winding faults in induction motors using three-phase current monitoring. *ISA Trans.* **2011**, *50*, 14–20. [CrossRef] [PubMed]
14. Ilamparithi, T.C.; Nandi, S. Detection of eccentricity faults in three-phase reluctance synchronous motor. *IEEE Trans. Ind. Appl.* **2012**, *48*, 1307–1317. [CrossRef]
15. Bacha, K.; Salem, S.B.; Chaari, A. An improved combination of Hilbert and Park transforms for fault detection and identification in three-phase induction motors. *Int. J. Electr. Power Energy Syst.* **2012**, *43*, 1006–1016. [CrossRef]
16. Ngote, N.; Guedira, S.; Cherkaoui, M.; Ouassaid, M. A New Hybrid "Park's Vector—Time Synchronous Averaging" Approach to the Induction Motor-fault Monitoring and Diagnosis. *J. Electr. Eng. Technol.* **2014**, *9*, 559–568. [CrossRef]
17. Elbouchikhi, E.; Amirat, Y.; Feld, G.; Benbouzid, M. Generalized likelihood ratio test based approach for stator-fault detection in a PWM inverter-fed induction motor drive. *IEEE Trans. Ind. Electron.* **2018**, *66*, 6343–6353. [CrossRef]
18. Sabir, H.; Ouassaid, M.; Ngote, N. Detection of an Incipient Rotor Winding Inter-Turn Short Circuit Fault. In Proceedings of the 2021 IEEE International Autumn Meeting on Power, Electronics and Computing (ROPEC), Ixtapa, Mexico, 10–12 November 2021; pp. 1–7.

19. Laadjal, K.; Sahraoui, M.; Alloui, A.; Cardoso, A.J.M. Three-Phase Induction Motors Online Protection against Unbalanced Supply Voltages. *Machines* **2021**, *9*, 203. [CrossRef]
20. Dongare, U.V.; Umre, B.S.; Ballal, M.S. Rotor winding inter-turn short-circuit fault detection in wound rotor induction motors using Wing Technique. *J. Power Electron.* **2022**, *22*, 614–628. [CrossRef]
21. Fortescue, C.L. Method of symmetrical co-ordinates applied to the solution of polyphase networks. *Trans. Am. Inst. Electr. Eng.* **1918**, *37*, 1027–1140. [CrossRef]
22. Suo, L.; Liu, F.; Xu, G.; Wang, Z.; Yan, W.; Luo, A. Improved Park's Vector Method and its Application in Planetary Gearbox Fault Diagnosis. In Proceedings of the 2018 IEEE International Conference on Prognostics and Health Management (ICPHM), Seattle, WA, USA, 11–13 June 2018; pp. 1–7.
23. Wang, Y.-J. Analysis of effects of three-phase voltage unbalance on induction motors with emphasis on the angle of the complex voltage unbalance factor. *IEEE Trans. Energy Convers.* **2001**, *16*, 270–275. [CrossRef] [PubMed]
24. Amlinger, H.; Arteaga, I.L.; Leth, S. Impact of PWM switching frequency on the radiated acoustic noise from a traction motor. In Proceedings of the 2017 20th International Conference on Electrical Machines and Systems (ICEMS), Sydney, NSW, Australia, 11–14 August 2017; pp. 1–6.
25. Feng, L.; Yang, H.; Song, W. Acoustic noise of induction motor with low-frequency model predictive control. *IEEE Access* **2020**, *8*, 178238–178247. [CrossRef]